Performance of NCAR Ka-band Radar During WISP04

July 2004

Vivek, Frank Pratte, R. Rilling, S. Ellis and Marcia K. Politovich

Table of Contents

Performance of NCAR Ka-band Radar During WISP04

1. Introduction

A dual-wavelength S- (2.8 GHz) and K_a-band (35 GHz) radar system with matched resolution volume and sensitivity was built to detect supercooled liquid droplets remotely. The detection of liquid water content was based on the principle that the shorter of the two wavelengths is more strongly attenuated by liquid water. ATD completed the initial development of a scanning Doppler millimeter wave K_a-band (35 GHz) radar using funds from the FAA and the NSF. The radar system was deployed during the Winter Icing Storms Project 2004 (WISP04) near Boulder, CO, to detect and estimate liquid water content (WISP04 project was funded by the FAA). Observations by dual-wavelength radar were collected in both non-precipitating and lightly precipitating clouds. The addition of the K_a-band system to the S-Pol created a system known as S-PolKa. There were several known problems with S-PolKa data and during WISP04. This report describes performance of the radar, its characteristics, sensitivity, and data quality. However, it should be noted that a few of the performance issues are not yet fully documented, nor are they perhaps yet fully understood. We acknowledge that the evaluation of Ka-band performance is an on-going task.

2. System Layout

One of the main design objectives of the S-PolKa radar was to match the K_a-band antenna with the S-Pol beamwidth and point the beams at the same direction simultaneously. In addition to ensuring matched beams, i.e., common radar sampling volume and a simpler scanning procedure for a dual-wavelength measurement, it was imperative that both S and Ka-band systems should have similar sensitivity. The following is a preliminary list of K_a-band parameters that were selected as the initial design parameters.

Table1: Preliminary design specification

	S-Band	KA-Band
Frequency	2809	35000
Wavelength	10.7 cm	.8 cm
Beamwidth	.93 deg	.93 deg
Antenna Diameter	8.5 m	.7 m
Antenna Gain	45 dB	45 dB
Peak Transmit Power	560kw (87 dBm)	33kw (75 dBm)
PRF	420 (H or V)	840
Unambiguous Velocity	22 m/s	.9 m/s
Pulse Width	1.0	.5 to 1.0
Radar Constant	68.5	59.1
Noise Power	-115 dBm	-110 dBm
MDS 0dB s/n @50km	-12 dBz	-16 dBz
Digital IF	Yes	Yes

The final K_a-band system parameters are slightly different from the initial specification due to changes in transmitter and waveguide characteristics as shown in Table 2.

Nominal K_a-band Radar Parameters for the configuration that existed 02 April 2004.

Table2: Current system specification

Predicted Blue Sky Noise Power in 1MHz Bandwidth dBm	-112.1
Carrier Frequency GHz	34.9
Pulse Width microseconds	0.8
Peak Power Watts	11980.0
Antenna Gain dB	45.2
Half-Power Beamwidth degrees	1.0
Fixed Losses (filter mismatch) dB	2.8
Meteorological Radar Constant (|K2|=0.93)	66.0
MDZe at 30 km dBZ	-16.6

The measured blue sky noise values for 3 days with the 3 magnetrons used during WISP04 were as follows: 23 February = -115.5 dB, 10 March = -112dB, 02 and April = -111.5dB.

A K_a-band radar antenna with the same 3-dB beam width as S-Pol was mounted on the S-Pol pedestal. Since the K_a-band frequency is 12 times larger, the antenna is 1/12 of the size of the S-band antenna. The receiver, low-noise amplifier, and circulators were located close to the K_a-band reflector antenna. The transmitter unit was mounted on the counterweight of the S-Pol antenna and a standard rectangular waveguide was used to channel the power to the antenna feed. The transmitter was built by Applied Systems Engineering in Boston and the antenna was built by the same company that manufactured the primary S-band antenna, Seavey Engineering Inc., Boston. No rotary joint is required for this configuration. Only a slip ring is used to connect with the main power supply. The K_a-band antenna is in the 8 o'clock position without blocking the view of the main S-Pol antenna.

Figure 1. S-Polka radar system at the Marshall field site near Boulder during WISP04 project.

The processed moments data (reflectivity, velocity and spectrum width) were transmitted via RF modem to the nearby radar van. The data were merged with the S-Pol data stream for a real time beam-by-beam display and recording. The merged data would simplify various product developments that use both dual-wavelength and S-band dual-polarization observations. The radar receiver uses a digital IF and a patented NCAR radar signal processor. The following set of variables was recorded:

CDBZ dBZ	S-band coherent reflectivity
DBZ dBZ	S-band reflectivity
DL dBm	S-band Vertical received power (co-polar: V-tx, V-rec)
DM dBm	S-band Horizontal received power (co-polar: H-tx, H-rec)
DX dBm	S-band cross-polar received power (H-tx, V-rec or VH)
DY dBm	S-band cross-polar received power (V-tx, H-rec or HV)
LDR dB	S-band depolarization ratio (H-tx, V-rec, or VH)
LVDR dB	S-band depolarization ratio (V-tx, H-rec, or HV)
LDR_VH_K dB	Ka-band depolarization ratio (H-tx, V-rec, or VH) (special note: H-polarization for Ka is often tipped up to 22 degrees off of horizontal)
NCP none	S-band normalized coherent power (HH)
NCP_HH_K none	Ka-band normalized coherent power (HH)
PHIDP deg	S-band differential phase
P_HH_KdBm	Ka-band co-polar received power (H-tx, H-rec or HH)
P_VH_K dBm	Ka-band cross-polar received power (H-tx, V-rec or VH)
RHOHV none	S-band Correlation coefficient between HH, VV
RHO_VH_K none	Ka-band Correlation coefficient between HH, VV
SW m/s	S-band co-polar spectrum width (computed from both SW_HH and SW_VV)
SW_HH_K m/s	Ka-band co-polar spectrum width (HH)
TH_VH_K deg	Ka-band differential phase (PHIDP of Ka) (not yet evaluated for utility)
VR m/s	S-band co-polar radial velocity (computed from both V_HH and V_VV using the CSU algorithms)
V_HH_K m/s	Ka-band co-polar radial velocity (HH)
ZDR dB	S-band differential reflectivity (DBZ_HH - DBZ_VV)
Z_HH_K dBZ	Ka-band co-polar reflectivity (HH)
NIQ dB	Average magnitude of backscatter pwr, HH
AIQ deg	Average phase of backscattered power (HH) AIQ is used in the Fabry refractive index work for the determination of virtual temp
CH none	Magnitude of cross correlation, HH and VH
AH deg	Angle of the cross correlation, HH and VH
CV none	Magnitude of cross correlation, VV and HV
AV deg	Angle of the cross correlation, VV and HV
KDP deg/km	[**Not Available**] Specific diff propagation phase (HH, VV)

3. Data collection

WISP04 ran from the mid-February 2004 to the beginning of April 2004, however, unfortunately, the weather did not cooperate for this project. There were several periods of system operation devoted to system tests, and other periods where forecasted weather did not materialize. Not all of the data collected is worth reviewing. It is recommended that the "quicklook images" be reviewed to determine if usable data exist for a particular time period. The following is a brief summary of the data:

- 19 February: light snow, drizzle
- 28 February: upslope cloud, some snow
- 29 February: snowstorm northeast of a line approximately FNL – FTG
- 4 March: heavy wet snow in northerly flow
- 10-11 March: stratiform upslope cloud with high liquid water content
- 27 March: rather patchy cloud
- 2 April: convection and notable K_a-band attenuation
- 3 April: stratiform, uniform cloud

The best case for the single wavelength and radiometer-based retrievals is 10 and 11 March, with a shallow, fairly uniform stratus cloud in the temperature range of ~ -5 to -15^{o}C, high liquid water content and little ice was found in the cloud. Strong ground clutter at the S-band observation may limit its usefulness for dual-wavelength application. This cloud began with some patches of higher reflectivity (~10-20 dBZ) and snow showers on the ground. It then evolved to low (<-10 dBZ) reflectivity and lots of liquid, as evidenced by numerous pilot reports of icing in the Denver area. K_a -band data were collected during two separate intervals due to the instability in the magnetron tube performance: (i) 10 March, 20:00-23:00; and (ii) 11 March, 1:30-3:00.

The 2-3 April measurements were made in drizzle and light rain. A variety of cloud microphysical characteristics was observed using both dual-wavelength and dual-polarization

systems. Precipitation likely was produced by both warm and cold rain processes. K_a-band and S-band radar systems were stable during this 24-hr long event. Even though no aircraft data were available, the dual-wavelength and radiometer observations can be used to develop algorithms to detect and estimate LWC in both non-Rayleigh and mixed-phase cloud conditions.

4. Analysis of K_a-band Radar

The design and development of K_a-band was a major challenge because it was the first millimeter wave radar built by ATD. New millimeter wave test equipment was acquired to diagnose the performance of the system. In order to meet the required measurement sensitivity, we decided to mount the system on the existing S-Pol antenna pedestal. Since no radome is used to protect the S-Pol antenna from changing weather conditions and precipitation, the K_a-band system required complete weatherproofing. In spite of the many changes to the original design plan, the system was completed in time for the project. However, the weatherproofing was inadequate and it affected the performance of the transmitter and receiver during wet snow and rain periods. Figures 2 and 3 show sample radar measurements during WISP04. Considering it is the first deployment for a newly developed radar system, its performance exceeded our expectations and met most of the initial requirements for the FAA project. However, additional improvements and upgrades to the system are planned to make the system more robust.

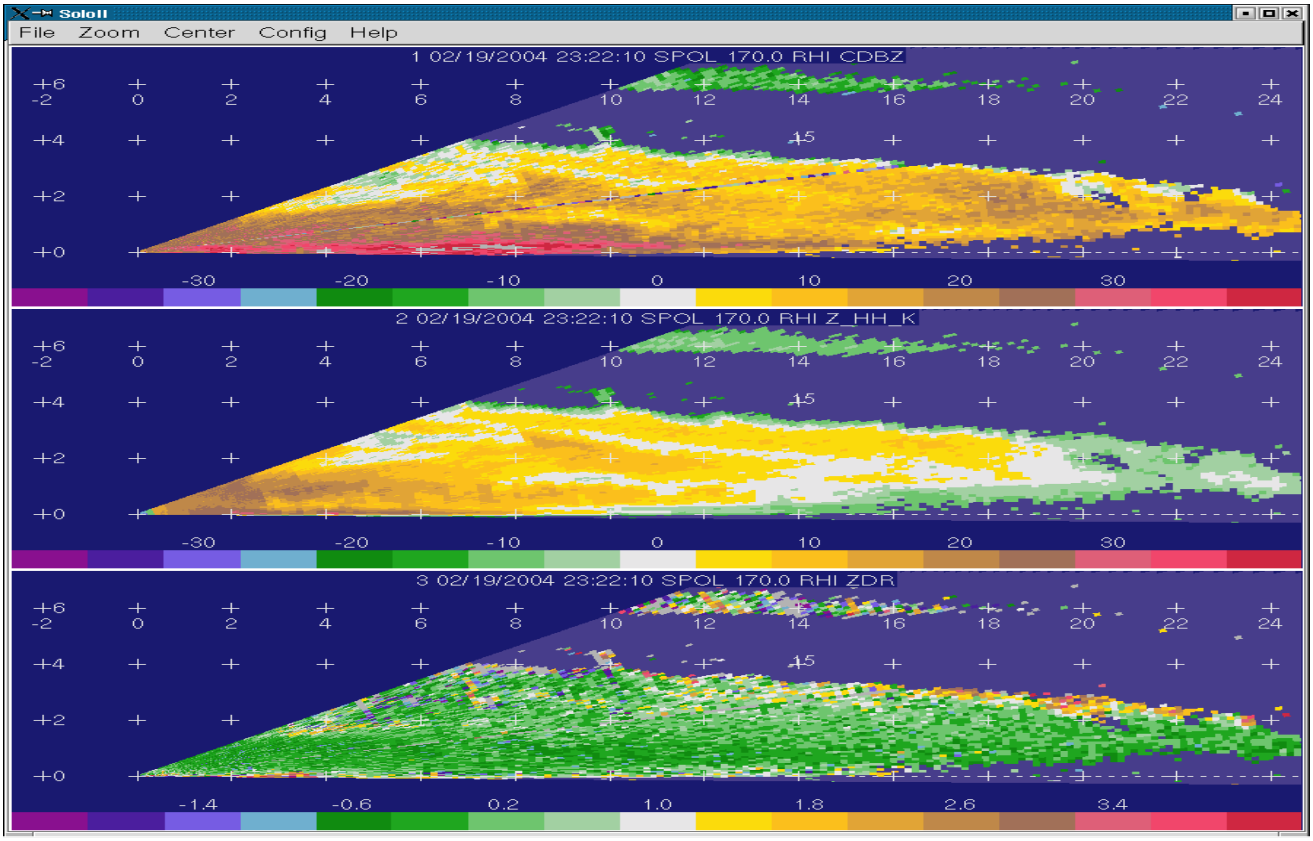

Figure 2. RHI scan of a winter precipitation. The top two panels are S and K_a-band reflectivities. The bottom-most panel show differential reflectivity at S-band. A thin cirrus layer at 6 km is composed of ice crystals. The 4 km deep precipitation is dominated by light snow and drizzle.

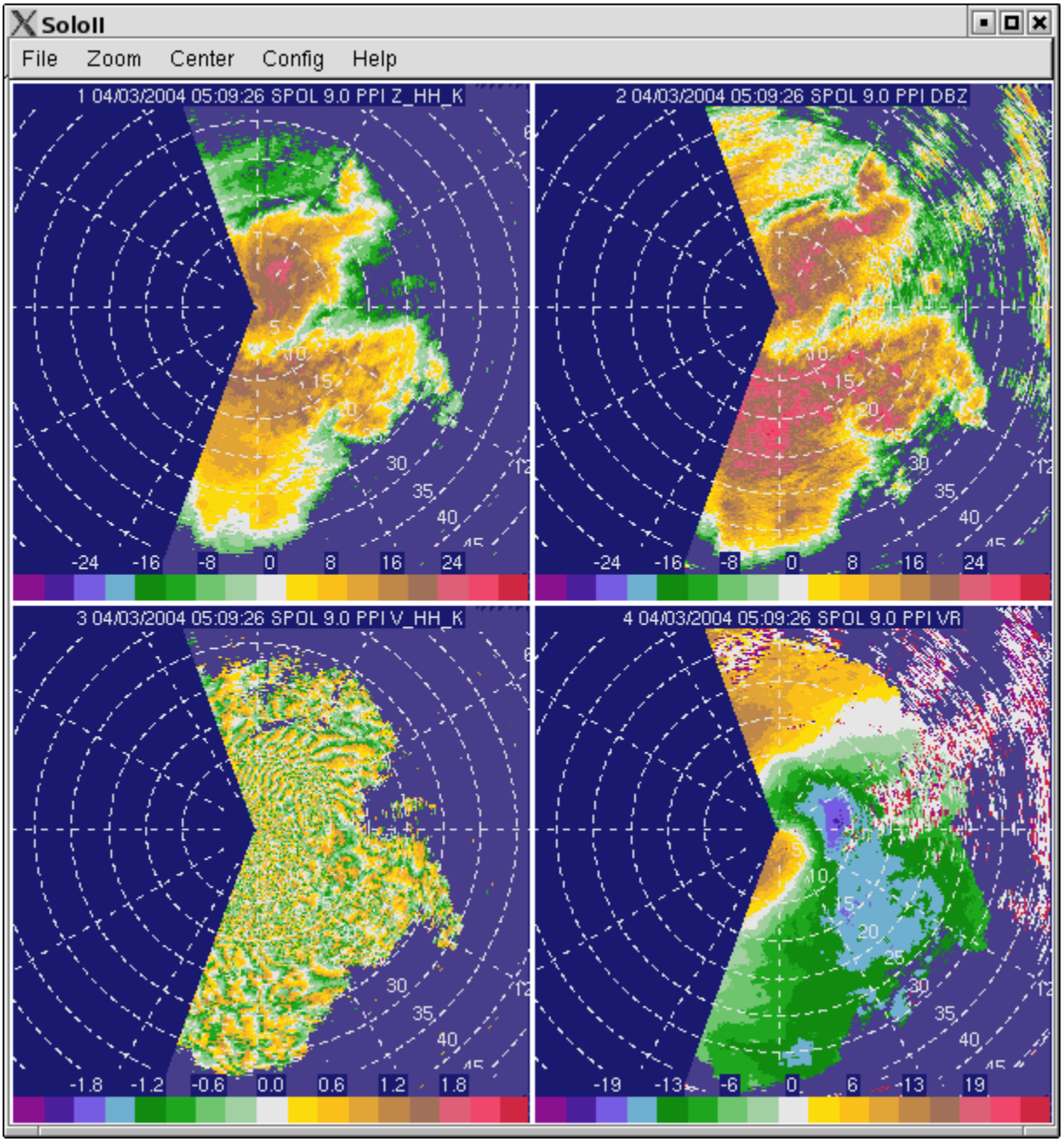

Figure 3. PPI scan of a light drizzle event. The decrease in K_a-band reflectivity (top left panel) relative to S-band reflectivity (top right panel along the radial, signify the attenuation of Ka-band signals due to liquid. The bottom two panels show radial wind observations at K_a- and S-bands. Low Nyquist at K_a-band cause folding even at 1 m/s. The S-band radial wind observation shows the regions contaminated by ground clutter. K_a-band observations are relatively immune to ground clutter due to its increased sensitivity to particle scattering cross-sections.

(a) Sensitivity

The following is a list of range (km) versus the minimum detectable blue sky reflectivity (MDdBZ) assuming standard conditions. The atmospheric gaseous loss at K_a-band is of 0.2 dB km^{-1} per 1g m^{-3} water vapor.

R(km)	MDBZe
5.0	-32.12
10.0	-26.10
15.0	-22.58
20.0	-20.08
25.0	-18.14
30.0	-16.56
35.0	-15.22
40.0	-14.06
45.0	-13.04
50.0	-12.12
55.0	-11.29
60.0	-10.54

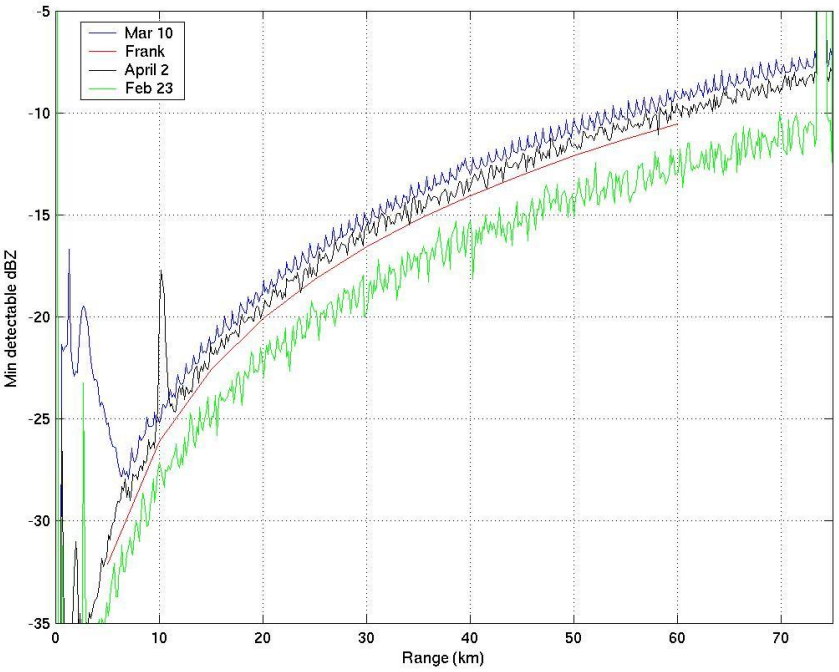

Figure 4. Plots of minimum detectable reflectivity (dBZ) for SNR = 0 dB. The red line is a plot of the values presented above, the other lines are plots of actual blue sky reflectivity measurements for the days indicated. These plots will likely change when the final data set is produced with all the known corrections applied.

(b) K_a-band Reflectivity Calibration

The absolute K_a reflectivity calibration is yet to be determined. Comparisons of K_a reflectivity to S-band reflectivity are ongoing. The changing-out of the magnetron for the K_a-band on about 30 March certainly affected any continuity in the calibration, as did other changes to the K_a-band system. Additionally, it is known that temperature changes had significant impact on the K_a-band receiver gain. Temperature also affected the K_a-band transmit frequency, a factor that could change the apparent received power if the frequency drifted outside of the K_a-band receiver bandwidth (the center of the pass band was designed to automatically adjust to the changing transmit frequency, but the effectiveness of this scheme needs to be evaluated).

(c) Data Recording

The S-Pol and K_a-band data streams are initially two independent streams from two separate data processors. The data from each has to be combined, with beams carefully matched between the two systems. For this matching, the only housekeeping parameter common to the two data streams is GPS time, since the K_a-band lacks information on pointing angles.

The initial data combination performed well enough in real time, but problems were found during post-processing, where the effective data rate was very high. For those cases, the housekeeping information had a tendency to become separated from the corresponding gate data, resulting in odd results where ground clutter features might be shifted from known locations, or segments of scans might be introduced into scans at other fixed-angles.

The data reconstruction problem has apparently been corrected, but users should avoid incorporating the original real-time data into any critical analyses and use the re-generated data instead.

(d) Beam Mismatch

A detailed review shows that the S-band and K_a-band radar beams on the S-Pol match closely in space and time. Some problems need correcting, and will be fixed in the final data set. The preliminary data have a mismatch of about 1° azimuth between the S and K_a-band beams, and one gate in range.

The matching of gates/beams between the two systems requires that:

- antennas must be physically aligned
- beams must start and end at exactly the same times
- internal processor delays must be accounted for to match gates in range

The independent radar system timestamps are based on GPS clocks combined with highly stable, disciplined oscillators slaved to the GPS time. This ensures that time can be accurately subdivided into tens of nanoseconds and that the clocks between the systems are in sync. To synchronize the triggering of transmit pulses and matching of dwells (beams), it is required only that the two systems have pulse repetition times (or pulse repetition frequencies) that are integer multiples of each other.

The K_a and S-band timestamps maintain their identity and are available for review after the combination of the two data sets. A review of these timestamps shows that the closest-matched beam times are consistently within 2.5 milliseconds of each other. Matched times were checked for subsets of data on every day of significant interest. Since both the K_a and S-band Horizontal PRF were 500 Hz and beams typically had 100 samples/beam with a rotation rate on the order of 5°/sec, there is an implied azimuthal match of +/- .025°.

This accuracy of beam matching was not borne out in a preliminary data review, as evidenced by a pronounced up/down shifting of K_a -band echoes during RHI scans (also CW/CCW shifting during PPIs). Extensive analysis, followed by a review of the radar system processor code, determined that the problem was related to the S-band timestamp being applied at the start of a beam, whereas the K_a-band timestamp was applied at the end of each beam. The net result is a one-beam shift in K_a-band data upon changes in direction. This problem exists in the preliminary project data set, and will be corrected only after the appropriate software change is made.

Further work was done in comparing azimuth and ranging using ground targets. The BAO and Fredrick towers provided good echoes with known azimuths and ranges. Careful review of the specially-collected slow and fast scan data, along with the analysis of individual gate values indicates that:

- S-band range needs to be corrected by one gate (move data one gate outward).
- Azimuthal accuracy of S-band is better than +/- 0.2°.
- The K_a and S-band antenna alignment matches to within 0.2° azimuth.
- Alignment of the K_a and S-band beams in elevation looks good, but could not be quantified.

Note that there is some suggestion that, independent of beam timestamp issues, the K_a-band antenna may be aligned 0.1° or 0.2° to the right of the S-band antenna (this implies that the K_a echoes tend to appear to the *left* of S-band echoes). Further review should be done after the beam timestamp matching is fixed.

(e) Transmitter Problem

The K_a magnetron failed part-way through the project and the change-out caused an error in the K_a-band calibration. K_a-band worked until 5 March 2004 at 0130Z. This was the first magnetron failure and the K_a-band was back in operation with a repaired tube on 10 March 2004. The operation was not very stable until a hard failure on 11 March 2004 at 0309Z. The stability

was suspect due to the magnetron not firing on every pulse. The output power was fluctuating resulting in poor data quality.

The K_a-band was back in service on 24 March 2004 with a new magnetron from Radio Research with the pulse width reduced from 840ns to 800ns. The PRF was the same 500 Hz. From this point until the end of WISP04 on 3 April 2004, the K_a-band transmitter operated in a stable mode with no further problems.

(f) Antenna-Pattern Measurements

On 31 March 2004, antenna-pattern measurements were conducted for both S and K_a-band radars. Two polarized horns were mounted at the NCAR Mesa Lab, one at S-band and the other at K_a-band. The K_a-band antenna was mounted horizontally for the pattern measurements. The horns were directed to maximize the bore-sight co-polar signal and then leveled by searching for the null in the cross-polar signal, along the bore-sight. The horns were then scanned by S-Polka to receive only mode, to obtain the antenna-pattern measurements. For each wavelength, measurements were made with the horns aligned both horizontally and vertically. The scanning strategy obtained a high resolution of 0.2 deg in both azimuth and elevation angles. The test signal was injected into the K_a-band measurements in order to correct for receiver drift due to temperature affects.

The data for a volume pattern measurement were combined in the following manner. First, a range average along each beam was computed. Second, the maximum co-polar value was subtracted from both the co- and cross-polar powers, resulting in fields that are relative to the co-polar power along the bore-sight. Third, the data were interpolated to a 2-D Cartesian grid with the X-axis representing azimuth angle and the Y-axis representing the elevation angle. The interpolation used was a cubic fit preserving the measured values. The standard Matlab contouring routine was then used to plot the pattern measurements. It should be noted that the one beam azimuth offset in the K_a-band was compensated for by adding or subtracting one beam

width (0.2 deg) from each PPI depending on which way the radar was scanning. Figure 5 shows the S and K_a-band horizontal co-polar pattern measurements. The contour interval is 3 dB.

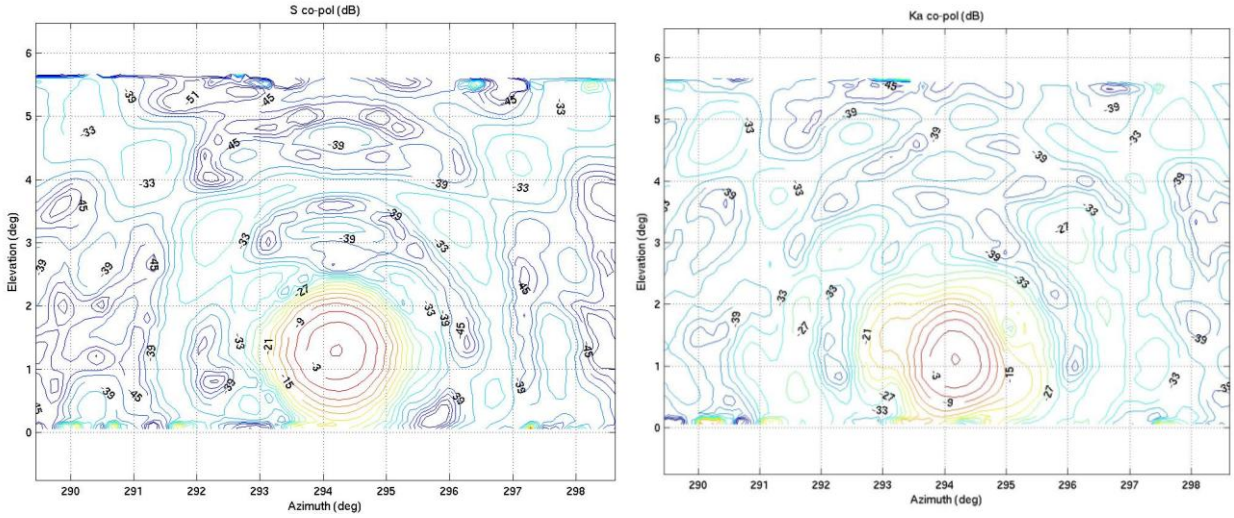

Figure 5. Co-polar antenna pattern measurements for S-band (left panel) and K_a-band (right panel).

The sidelobes from the antenna struts are evident at 45 degree angles from the bore-sight for both radars (Figure 5). The maximum measured sidelobe for S-band was –27.7 dB and for K_a -band was –27.0 dB. To obtain these estimates, only the sidelobes in the upper half of the antenna pattern were considered to avoid increased contamination from the ground at low elevation angles.

The half-power beamwidths for the K_a-band were estimated using the antenna-pattern measurement. The beamwidth in azimuth was 0.81 degrees, 0.92 degrees in elevation and 0.87 degrees total. It can be seen from Figure 5 that the center of the beams for the K_a and S-band radars are offset in elevation angle by approximately 0.2 degree, in agreement with the pointing and ranging calibration performed earlier.

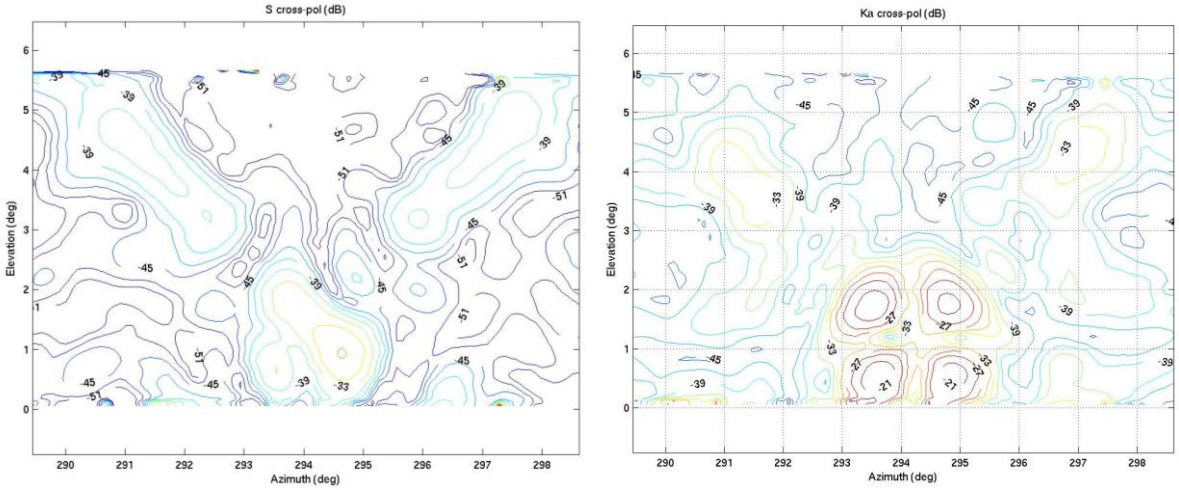

Figure 6. Cross-polar antenna pattern measurements for S-band (left panel) and K_a-band (right panel).

Figure 6 shows the S and K_a-band horizontal cross-polar pattern measurements. In this case the horns were aligned horizontally and the vertical received power is plotted. Again, the sidelobes from the struts are evident. In the cross-polar patterns the K_a sidelobes are much higher than the S-band sidelobes. The maximum side-lobe for the S-band pattern was –25.3 dB and –19.4 dB for the K_a-band. Cross-polar pattern measurements are very sensitive to contamination from multiple path echoes, small errors in horn alignment, etc. However, the high cross-polar sidelobes might be indicative of poor isolation between polarization states. This situation could result in the low sensitivity of the K_a-band LDR measurement observed during WISP04. An LDR limit of –15 dB was computed from the antenna pattern using the following integration:

$$LDR\_\lim = \frac{\int\int \left| \sqrt{Z_{VH} \cdot Z_{HH}} + \sqrt{Z_{VV} \cdot Z_{HV}} \right|^2 \cos\theta d\theta d\varphi}{\int\int \left(Z_{VH} + Z_{HH} \right)^2 \cos\theta d\theta d\varphi},$$

where Z_{TR} is power, the subscripts denote transmit and receive polarization states of H or V, and θ and ϕ are elevation and azimuth angles respectively. The integration was performed from the elevation angle of the bore sight to the top of the scan and then multiplied by two. This assumes the antenna pattern is symmetric but avoids including the stronger ground effects at the lower

elevation angles. The LDR limit result is in general agreement with the lowest measured LDR values in weather of about –18 to –20 dB, demonstrated in Figure 7. The top left and right panels of Figure 7 show K_a and S-band reflectivity respectively and the lower left and right panels show K_a and S-band LDR. The minimum LDR from S-band is approximately –26 dB while the K_a-band minimum is about –20 dB. The K_a-band co-polar transmitted wave was at a 22 degree angle with the vertical, so the LDR values won't necessarily correspond to the S-band values. However, lower values of K_a LDR would be expected in cloud or drizzle drops, but were never observed.

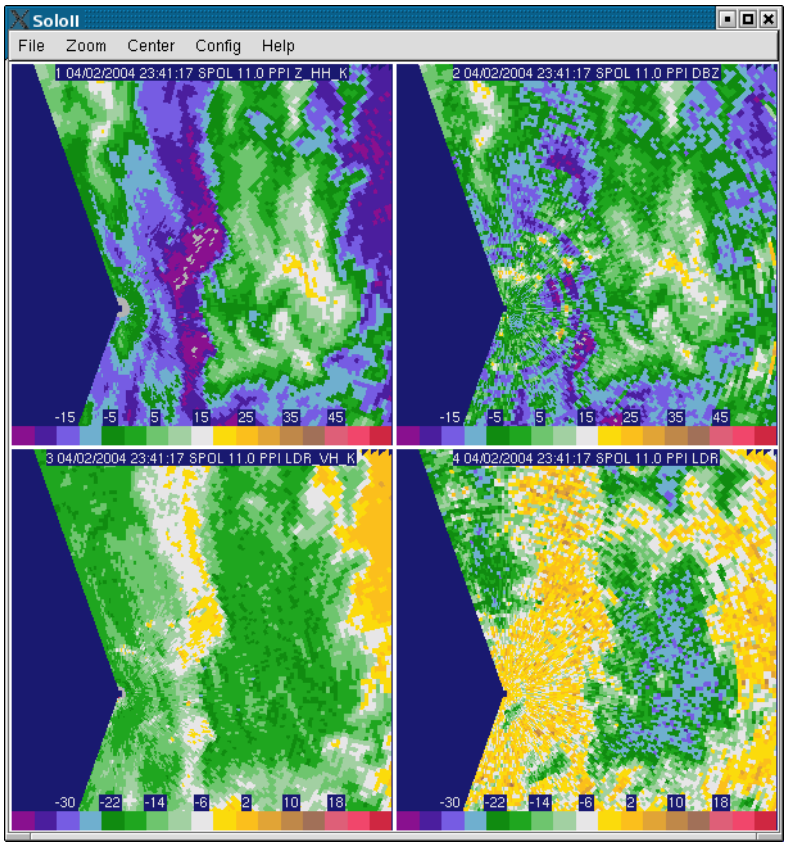

Figure 7. PPI scan of K_a-band reflectivity (upper left), S-band reflectivity (upper right), K_a-band LDR (lower left) and S-band LDR (lower right).

Further evidence of cross-talk between K_a -band polarizations can be seen by plotting the cross-correlation coefficient (ρ_{xh}) versus LDR, following Moisseev, et al. (2002). Figure 8 shows scatter plots of ρ_{xh} and LDR taken from Moisseev, et al. (2002) and collected from the K_a-band during WISP04. The data from both scatter plots were collected in precipitation with the antenna pointing vertically. The ρ_{xh} should be near zero for large values of LDR (around –15) and show an increase as LDR decreases, as seen in the Moisseev, et al. (2002) plot. The value of ρ_{xh} would be unity for LDR = -∞. The desired trend is not observed in the K_a-band data. Furthermore, the average ρ_{xh} value for an LDR of –13 dB is around 0.34, roughly 3 times that for a comparable LDR from Moisseev, et al. (2002).

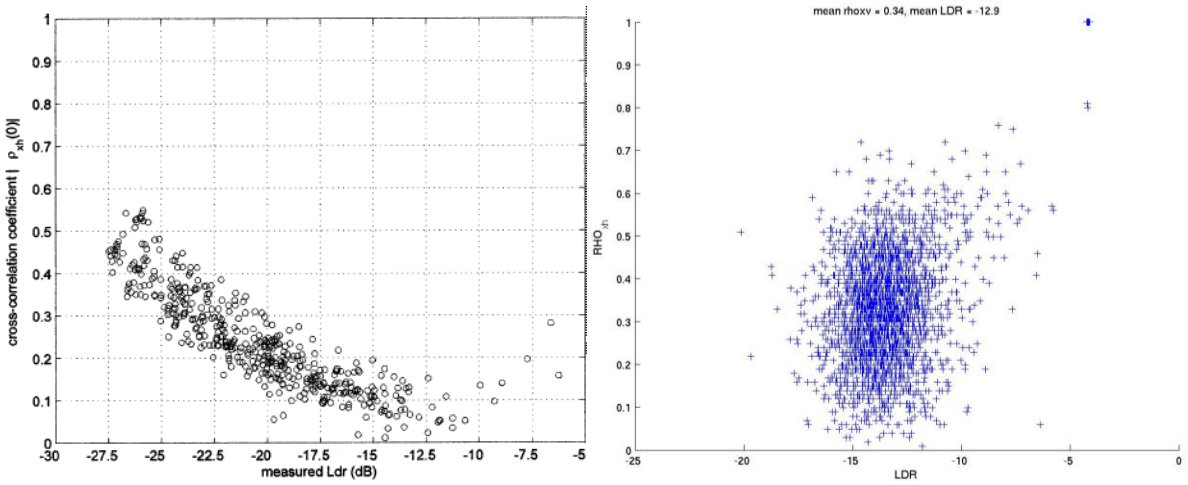

Figure 8. Scatter plots of cross-correlation coefficient and LDR from vertical pointing measurements in precipitation, taken from Moisseev, et al. (2002) (left panel) and measured with the K_a-band radar during WISP04 (right panel).

5. Proposed Upgrade to Reliability and Performance of Ka-band Radar

(a) Hardware Upgrades

There were two major issues concerning the K_a-band performance that surfaced during WISP04: (i) potentially-low system availability (reliability) due to the component failures, and (ii) the stability of displayed reflectivity (and thermal noise floor), which seemed to vary

noticeably from hour-to-hour during the experiment. These observations and areas of concern imply a similar performance during RICO, unless dealt with. System availability may be improved in various ways; however, the practical way to do this for RICO is to purchase additional spares as listed below that will reduce the time used to repair. The following is a list of spares:

Magnetron for Transmitter (from Radio Research) . $15k
MMW Frequency Synthesizer ……. $6k
IF Frequency Synthesizers ……. $2k
Amplifiers (assorted) …… $4k
Trigger Interface Board …….. $1k
Transmit/Receive tube ……..... $9K
Total cost of spares is ……. $37K

The K_a-band operations, during the WISP04 indicate that the transmitter and receiver require the following critical enhancements: (i) the incidence of heat-related problems with the transmitter can be minimized by reducing peak temperatures in the transmitter, and (ii) variations in displayed reflectivity appear to originate from uncompensated thermal changes in processor and receiver gain. The following components are required for the transmitter and receiver upgrades:

High Capacity Heat Exchanger for Transmitter Enclosure……$4K
Sunshield(s) for Transmitter Enclosure …… $2K
Medium Capacity Heat Exchanger for Processor Enclosure (reuse the current transmitter heat exchanger) ……-0-
Sunshield for Receiver Enclosure …… $1K
Thermal Control Plate for Receiver Enclosure Amplifiers …….. $2K
IF Dicke Switches …….. $1K
Total cost of parts for upgrade …….. $10K

These upgrades will improve the reliability and performance of K_a-band radar system. The prices given above are educated guesses which include overhead.

(b) Software Fix Required or WSP04 Data

1) K_a and S-Pol beams do not match in azimuth. The direction of mismatch changes with the scanning direction. This problem is likely due to S-band beams being timed at the start of the beam, whereas K_a are timed at the end of a beam. We need a routine that will time-shift the K_a data by one beam, and match it to the S-band beam.

2) S-Pol gate data do not match K_a gate data which is evident from the hard target studies. The S-band data needs to be moved outward by one (integer) gate.

3) The K_a-band HH noise power is in error in the K_a housekeeping, and has an impact on calculated values of K_a power (P_HH_K), which goes into K_a reflectivity (Z_HH_K). Housekeeping shows a noise power of -110.0 and -110.5 dBm. The best guess value is 112.1 dBm. This result makes a real difference at low-received power, and should be fixed. Note that the cross-polar K_a noise power is also in error.

4) Vertical pointing observations indicate that the S-band Zdr is biased by 0.08 dB and this value should be added all Zdr observations.

5) The K_a co-polar radar constant for the first portion of the experiment need to be corrected. The correction can be applied to Z_HH_K (similar to the Zdr correction at S-band), or use the revised radar constant to process the K_a-band reflectivity from measured backscattered power values.

6) One of the greatest challenges will be an adjustment of Z_HH_K based on an expected P_HH_K test pulse power, combined with an automatic analysis of a sweep-by-sweep variation from that nominal value.

6. Summary

The preliminary analysis of K_a-band reveals that it is capable of detecting cloud droplets within a 30- to 40-km range, but in order for it to perform at full capacity, upgrades are required. Even though the primary objective of the FAA project is to detect and estimate cloud liquid and drizzle, a number of NSF scientists have shown a keen interest in using the 35 GHz radar for a number of cloud microphysical studies.

The K_a-band was operated successfully during the WISP04 project, as it captured most of the weather events. However, it was not as robust as the S-Pol system. The data quality of S-band was compromised due to excessive clutter at the Marshall site. The radar was deployed at Marshall to ease the tight development schedule in the interest of completing the K_a-band system. Most of the known problems with the K_a-band data have been identified and the corrected data should be available to the user community by end of summer 2004.

A preliminary analysis of the data revealed that the combination of dual-wavelength (S and K_a-bands) and dual-polarization (horizontal and vertical) is integral to the detection of cloud liquid water and mixed-phase cloud. Attenuation measurements from S-Polka are directly related to quantitative precipitation estimation, such as liquid water content and rain rate. A dedicated dual-wavelength system, with matched resolution volume and sensitivity, would further the remote sensing application in ground, airborne and space-based platforms.

7. Reference

Moisseev. DN, Unal, CMH, Russchenberg, HWJ, and Ligthart, LP, 2002: Improved polarimetric calibration for atmospheric radars. J. Atmos. Oceanic Tech., 19, 1968-1977.